A study on factors influencing the performance of CMFs on measurement of high viscosity flows

G. A. Dalson[a]* • B.C. Khoo[b] • L. Rongmo[c]

[a]University of Rwanda, Rwanda
[b]National University of Singapore, Singapore
[c]Xylem Water Solutions Pte Ltd., Singapore

Abstract: Coriolis Mass Flowmeters (CMFs), outperform other flow measurement systems owing to their perceived high accuracy and good repeatability. These have attracted their use in different fields including the bunkering industry. Bunkering operations entail high-viscosity flows that may limit the applicability of high-accuracy CMFs. Furthermore, their performance for measurement of single-phase high viscosity flow remains less explored and the mechanisms responsible for possible additional measurement error due to high viscosity fluid are not thoroughly studied. This study characterizes the performance of CMFs in the measurement of high-viscosity fluid via CFD simulations. It is observed that the error of CMFs on measurement of high viscosity is deemed relatively large at low mass flowrates and monotonically decreases as the viscosity decreases. The sudden pressure increase and the occurrence of secondary flow in the vicinity of the flow sensors' locations are the key factors influencing the measurement discrepancy. It is worth to note that this study is highly significant to the bunkering industry as it can serve as a baseline for further experimental works on the measurement of bunker fuel oils.

*Corresponding author.
E-mail address:* bwgace@gmail.com (G. A. Dalson).
Peer Review under the responsibility of Universidad Nacional Autónoma de México.

1. Introduction

Coriolis mass flowmeters (CMF) are supposedly some of the most accurate flow measurement devices (Reizner, 2005). Thus, they have been the most used measurement techniques for different industrial applications. Among other applications, CMFs are used to measure the density and viscosity of black liquor from pulp paper production (Dutka et al., 2004). In addition, CMFs are the primary measurement instruments in vanish production (Engelbert et al., 2007) regardless of the environmental conditions that the process entails (Mattar, 2003).

The aforementioned ability to maintain a high degree of accuracy and repeatability under challenging conditions enables CMFs to be widely adapted for use in the oil and gas industry for the measurement of Liquefied Natural Gas (LNG) (Basrawi, 2003) and fuel bunkering (Gregory et al., 2008). These are further pieces of evidence of the applicability of CMFs. However, still, bunker fuel entails high viscosities which may compromise CMF measurement accuracy. It has been shown that of all the fluid properties, fluid viscosity prominently and greatly hinders the performance of CMFs (Drahm & Bjonnes, 2003; Dutka et al., 2004; Kalotay,1994;1999). Moreover, studies have elucidated that most CMFs are plagued by relatively large inaccuracies at low Reynolds numbers (Rongmo & Jian, 2013). Noting that the operation of CMFs is supposed to be independent of fluid properties and flow speed (Cascetta, 1999; Kutin et al., 2006), it may be suggested that the observed underperformance of CMFs under low Reynolds numbers could be due to the fluid's high dynamic viscosity.

As a very first step towards the mitigation of CMFs' error due to fluid's viscosity, researchers opted for monitoring the variations of viscosity in an attempt to understand how the viscosity affects the measurement process and hence the measurement accuracy. In fact, Drahm and Bjonnes (2003) characterized the CMF by integrating it with viscosity measuring systems. They commented that CMFs, which are intrinsically multivariable devices when integrated with viscosity measurement acquire even more functionalities. Hence, they offer users better control over the overall process. This feature offers CMFs the capability to successfully measure fluids' viscosity. However, Kalotay (1999) who also provided a method of measuring the fluid viscosity using CMFs, remarked that the accuracy of CMF measurement can be compromised due to the use of multiple transducers attached that introduce additional uncertainties.

In addition to these studies that dealt with measuring the viscosity of the fluids and therefore controlling the operation of CMFs accordingly, other studies have been undertaken to explain how the fluid viscosity may limit CMFs' accuracy. Among others, (Cascetta, 1996; 1999) and Wang and Hussain (2010) suggested that pressure due to the high viscosity of the fluid may change the meter's response and induce extra measurement errors.

In addition to the rapidly rising pressure inside a CMF, researchers have also associated CMF error on the measurement of highly viscous flows to the distribution of the velocity field (Bobovnik et al., 2004; 2005; Hemp, 2002; Kumar et al., 2010; Kutin et al., 2005; Kutin & Bajsić, 2001), while others contradicted that and argued that the uncertainties due to velocity profile/distribution on the meters' performance became negligible in the currently available CMFs (Bobovnik et al., 2004).

It is clear that the error on CMFs' performance due to the viscosity of the fluid being metered remains at best only partially understood. Moreover, the fluid dynamics associated with that error need to be carefully studied. Hence, this study carries out a quantitative investigation of the influence of the fluid's viscosity on the performance of CMFs at the current state of CMF technologies via CFD simulations. Furthermore, it explains the potential fluid dynamics associated with the change in viscosities that affect CMFs performances.

2. Materials and methods

2.1. Model analysis
The modal analysis was carried out to determine the natural frequency and corresponding modal shape at which the CMF should be forced to oscillate. Modal frequencies are usually obtained by solving the standard Eigenvalue equation (2.1).

$$M\ddot{x} + C\dot{x} + \mathcal{K}x = F(t) \tag{2.1}$$

where for a CMF, the external exciting force $F(t)$ is
$$F(t) = F_0 \sin(2\pi n f_d \Delta t). \tag{2.2}$$
Here, M, C, and $\mathcal{K}$ are the Mass Matrix, Damping Matrix, and Stiffness Matrix, respectively. F_0 is the amplitude of excitation force, f_d is the first natural frequency of the CMF while Δt is the time shift between the oscillations of the sensors.

2.2. Structure domain
The structure's motion is modeled by Hamilton's variational principle, equation (2.3) as in (Rongmo & Jian, 2013). It provides full information on the system's dynamics by the use of an action integral of a single function.

$$\int_{t_1}^{t_2} \delta \left(W_P - W_k \right) dt = 0 \tag{2.3}$$

where W_P and W_k are total potential energy and total kinetic energy. They are respectively represented by equations 2.4 and 2.5 (Mole et al., 2008).

$$W_P = \frac{1}{2}\int \sigma_s.\, \varepsilon_s d - \int \vec{p}_s.\, \vec{x}_s d\Gamma_s \\ - \vec{F}(t).\, r_p \tag{2.4}$$

$$W_P = \frac{1}{2}\rho_s(\vec{v}_s.\, \vec{v}_s)\, dV_s \tag{2.5}$$

where $\vec{p}_s(x,t)$ the surface tractions acting upon the moving shell boundary through the respective displacement $\vec{x}_s(x,t)$ and $F(t)$ is the driving force. $\varepsilon_s(x,t)$ and $\sigma_s(x,t)$ are the strain and the stress tensor in the structure, and r_p is the position vector of the point where the force $F(t)$ is applied. ρ_s is the structure material density and $\vec{v}_s$ is the structure velocity field.

2.3. Fluid domain

The governing equations for the fluid domain are the Reynolds-averaged Navier-Stokes (RANS). For the incompressible steady-state flow as follow, they are presented as equations (2.6) and (2.7):

$$\frac{\partial(\overline{\rho_F u_i})}{\partial x_i} = 0 \tag{2.6}$$

$$\frac{\partial}{\partial x_j}(\overline{\rho_F u_i u_j}) = -\frac{\partial \overline{P}}{\partial x_i} + \frac{\partial}{\partial x_j}\left[\mu(\frac{\partial \overline{u}_i}{\partial x_i} + \frac{\partial \overline{u}_j}{\partial x_i} - \frac{2}{3}\,\delta_{ij}\frac{\partial \overline{u}_l}{\partial x_l})\right] \\ + \frac{\partial}{\partial x_j}(-\overline{\rho_F u_i' u_j'}) \tag{2.7}$$

where $\overline{u}$ is the mean (streamwise) velocity of the fluid, u' is the turbulence fluctuations, $\overline{\rho}_F$ is the average density of the fluid, $\overline{P}$ is mean pressure, μ is the dynamic viscosity and $\overline{\rho_F u_i' u_j'}$ is the Reynolds stresses.

2.4. Key parameters

The deformation (difference of displacement) of the meter (Δz_{CMF}) can be calculated by equation (2.8).

$$\Delta z_{CMF} = \Delta d_{CMF} = \vec{\omega}x\vec{v}.\, \Delta t^2 \tag{2.8}$$

where Δt is the time shift between the oscillation of the inlet and outlet sensor points.

The time shift corresponding to the displacement at the locations of sensors (at the sensor at the inlet arm and the sen-

sor at the outlet arm) is used to determine the mass flowrates of the fluid through the CMF. That is,

$$\dot{m} = K.\, \Delta t \tag{2.9}$$

where

$$K = \frac{k_s L}{8r^2} \tag{2.10}$$

Here, K is the meter factor, L is the length of the CMF arm to the sensor and r is the radius of curvature of the CMF arm.

2.5. Modeling and simulation

This study considered a 3D CFD model of a U-shape CMF made of 316L stainless steel in Figure 1 for which properties are presented in Table 1. The volume of a single tube is $2.5368 \times 10^{-0.005} m^3$, while its mass is 0.20472 kg.

The model analysis was conducted by using a mechanical ANSYS Parametric Design Language (ADPL) solver. The CMF's tube was clamped at both ends and allowed to undergo free undamped oscillations. As a result of fixing the inlet and the outlet, the number of degrees of freedom for the tube reduces to 6.

The exciter was used to force the CMF's tube to undergo undamped oscillations into the appropriate modal shape. These oscillations caused by the excitation force induce symmetric displacements of the CMF. Two motion sensors (S1 and S2 in Figure 1) were mounted symmetrically to the point where the excitation force is applied to detect and display these displacements.

For the fluid domain, FLUENT software was used. The Shear Stress Tensor k-ω turbulent model was chosen to solve the Reynolds-averaged Navier-Stokes (RANS) equations 2.6 and 2.7. Among the RANS turbulence models, the Shear Stress Tensor (SST) k- ω is deemed the most accurate and powerful. It combines the accuracy of the k-ε model in the free stream region and the excellent performance of a k- ω in the near-wall region.

Throughout the simulations, the velocities had been repeatedly varied at the inlet. The initial velocities corresponding to the selected sample of mass flowrates are presented in Table 2. In the table, NFR stands for nominal flowrate and ID is the inner diameter of the meter's tube. For the current study, 14 different inlet velocities were considered. After separately carrying out simulations on structural dynamics and fluid dynamics both the dynamics were coupled to simulate the dynamics of the combined fluid-tube system.
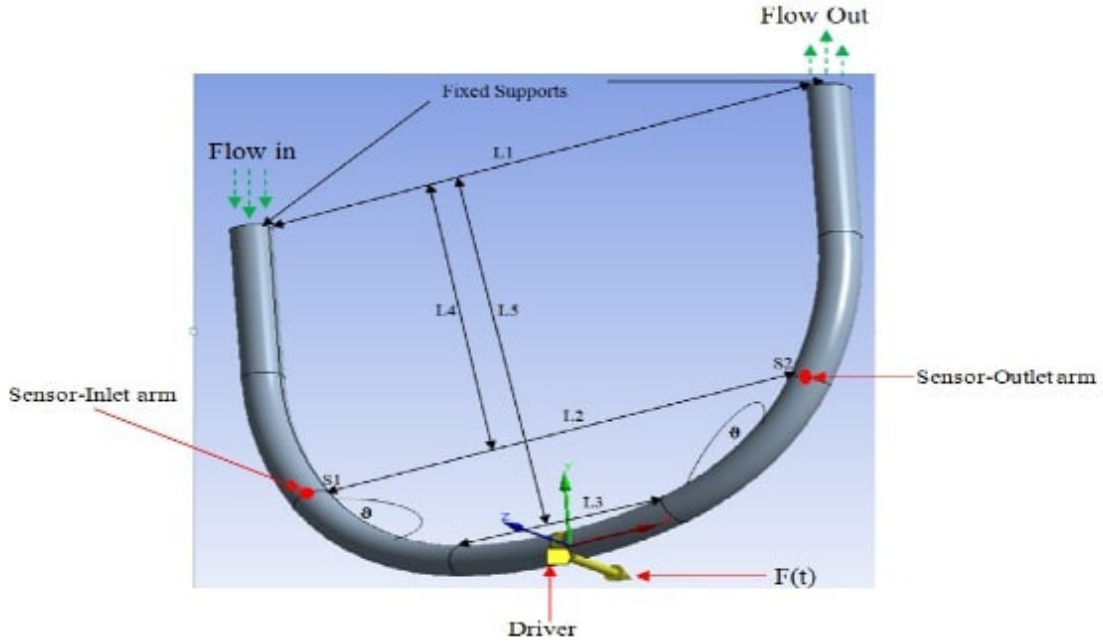
Figure 1. CFD model of a U-shape tube.

L1, L2, L3, L4, and L5 are lengths of different sections of a CFM, θ is the angle of bend of the CFM pipe while FM. The excitation force F(t) is indicated by a yellow arrow in the z-direction.

Table 1. Dimensions and properties of the CMF tube.

Dimensions	L1=364.090mm	L2=310.560mm	L3=131.120mm	L4=274.466mm	L5=396.252mm	ϑ=144.24⁰C
Properties	$\rho = 8070$ kg/m³	Bulk Mod. 16x10⁻⁶/K	Young Mod. $= 2x10^{11}$ Pa	P. Ratio= 0.3	Bulk Mod. = 1.67$x10^{11}$ Pa	Shear Mod.= 7.68x10¹⁰ Pa

L1 to L5 are the lengths of the meter tube's segments as defined in the preceding section while ρ_s is the density of the tube.

Table 2. Inlet velocities.

NFR (kg/min)	ID (mm)	Density (kg/m3)	Velocities (m/min)	Velocities (m/sec)	V 1CMF (m/sec)
50	28	1000	81.17	1.35	0.68
60	28	1000	97.40	1.62	0.81
100	28	1000	162.34	2.71	1.35
150	28	1000	243.51	4.06	2.03
151	28	1000	245.13	4.09	2.04
200	28	1000	324.68	5.41	2.71
250	28	1000	405.84	6.76	3.38
300	28	1000	487.01	8.12	4.06
350	28	1000	568.18	9.47	4.73
400	28	1000	649.35	10.82	5.41
450	28	1000	730.52	12.18	6.09
500	28	1000	811.69	13.53	6.76
540	28	1000	876.62	14.61	7.31
600	28	1000	974.03	16.23	8.12

3. Results and discussion

3.1. Mass flowrates and meter error

The simulations were carried out on water with μ=0.001003 kg/m.s and ρ=998.2 kg/m³, Fuel Oil with μ=0.048 kg/m.s and ρ=960 kg/m³, Engine Oil with μ=1.06 kg/m.s and ρ=889 kg/m³, RME180 with μ=0.17838 kg/m.s and ρ=991 kg/m3, and RMG380 with μ=0.37658 kg/m.s and ρ=991 kg/m3. The temperature was kept at 27°C. The resulting mass flowrates are presented in Table 3. According to the table, the computed mass flowrates differ slightly from the baseline and there is no case

in which the estimated mass flowrates are above the actual mass flowrates observed.

By a closer investigation of the error presented in Figure 2, the simulation predicts the error on computed mass flowrates that sharply decreases as the NFRs increase. For example, for Engine Oil with dynamic viscosity, μ=1.06 kg/m. s and density ρ=889 kg/m³, the error has decreased by about 65% as the mass flowrates increased from 50 kg/min to 600 kg/min. The change in density has no significant influence on the result. As can be noted, the deviation for RME180 with μ=0.17838 kg/m. s and ρ=991 kg/m³ and RMG380 with μ=0.37658 kg/m. s and ρ=991 kg/m³ differ despite having the same density.

Table 3. Computed mass flowrates for fluid with different viscosities.

| NFR (kg/min)	Fuel Oil	Engine Oil	RME180	RMG380
	MFR (kg/min)	MFR (kg/min)	MFR (kg/min)	MFR (kg/min)
50	47.96	44.39	48.62	47.84
100	96.94	91.42	97.94	96.17
150	145.63	138.76	147.07	144.58
200	194.38	188.27	196.38	193.60
250	243.10	236.46	246.00	242.34
300	292.20	285.34	295.77	292.24
350	340.88	334.02	345.73	341.74
400	389.61	382.60	395.43	390.89
450	438.56	431.16	445.07	440.94
500	487.83	479.33	494.55	490.09
550	537.77	527.88	544.85	539.71
600	587.14	576.39	594.50	589.24
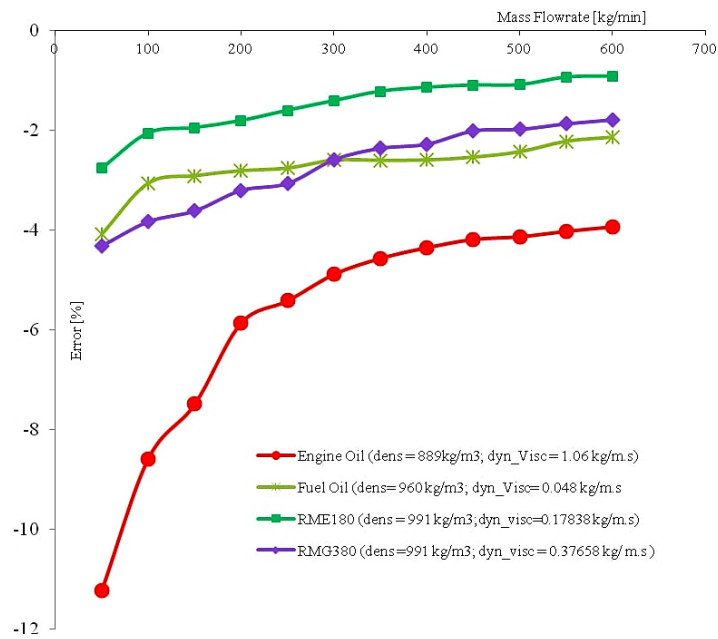
Figure 2. Errors in mass flowrates.

3.2. Sudden pressure increase

The sudden variation of pressure on the walls of the CMF's tube may be one of the main causes of error growth as the viscosity of the fluid increases. Figure 3 a-d plots the distribution of the total pressure on the walls of a CMF at each node from the inlet to the outlet. In Figure 3.a and Figure 3.c the pressures exerted by a highly viscous Engine Oil to CMF walls are plotted while in Figure 3.b and Figure 3.d the pressures exerted by water flow are presented. The dynamic viscosity of Engine Oil is 1.06 kg/m. s and is approximately 1000 times higher than the dynamic viscosity of water, i.e. 0.001003kg/m. s.

As can be seen from the figures, the pressures of the water flow on the CMF remain fairly evenly distributed. In this, the influence of pressure on CMFs' error remains as small as 0.01% to 0.13% per bar depending on CMF type/generation (Wang & Hussain, 2010). Unlike water flow, for the highly viscous Engine Oil, the pressure largely increases suddenly in the vicinity of sensors (between 40% and 60% of the CMF length where the driving force and the sensors are located). The impulsive change of pressure in the more sensitive part of the CMF tube (near the location of the sensor at the outlet arm) likely lead to the outsized measurement errors. The sudden increase of pressure is likely to be associated with the occurrence of secondary flow. Various studies found that the secondary flow occurs due to low Reynolds numbers. Particularly, this study found that the reverse flow potentially due to high viscosity causes a sudden pressure raise near the sensor at the outlet arm S2, see Figure1. When the flow reverses at the sensor S2, a part of the fluid returns towards the central part of the CMF mixing with the fluid flowing from the inlet causing the pressure surge in the section of the CMF just upstream of sensor 2 at the outlet arm as can be seen on Figure 3.a and Figure 3.c.

On the other hand, for water flow, the secondary flow of much lower magnitudes occurred in the central part of the tube, see Figure 4 and Figure 6. It is far from the sensors' locations compared to the locations where the secondary flow occurred for the high viscosity flows. This results in a significant variation in pressure between the sensor at the inlet arm and the sensor at the outlet arm of the CMFs as can be seen in Figure 3. b and Figure 3. d. However, that variation of pressure is very low and not sudden compared to the change of pressure observed for high viscosity engine oil flow (Figure 3. a and Figure 3. c). Hence the associated deviation in the CMFs readings is insignificant compared to CMFs' errors for measurement of high viscosity flow, Figure 2.
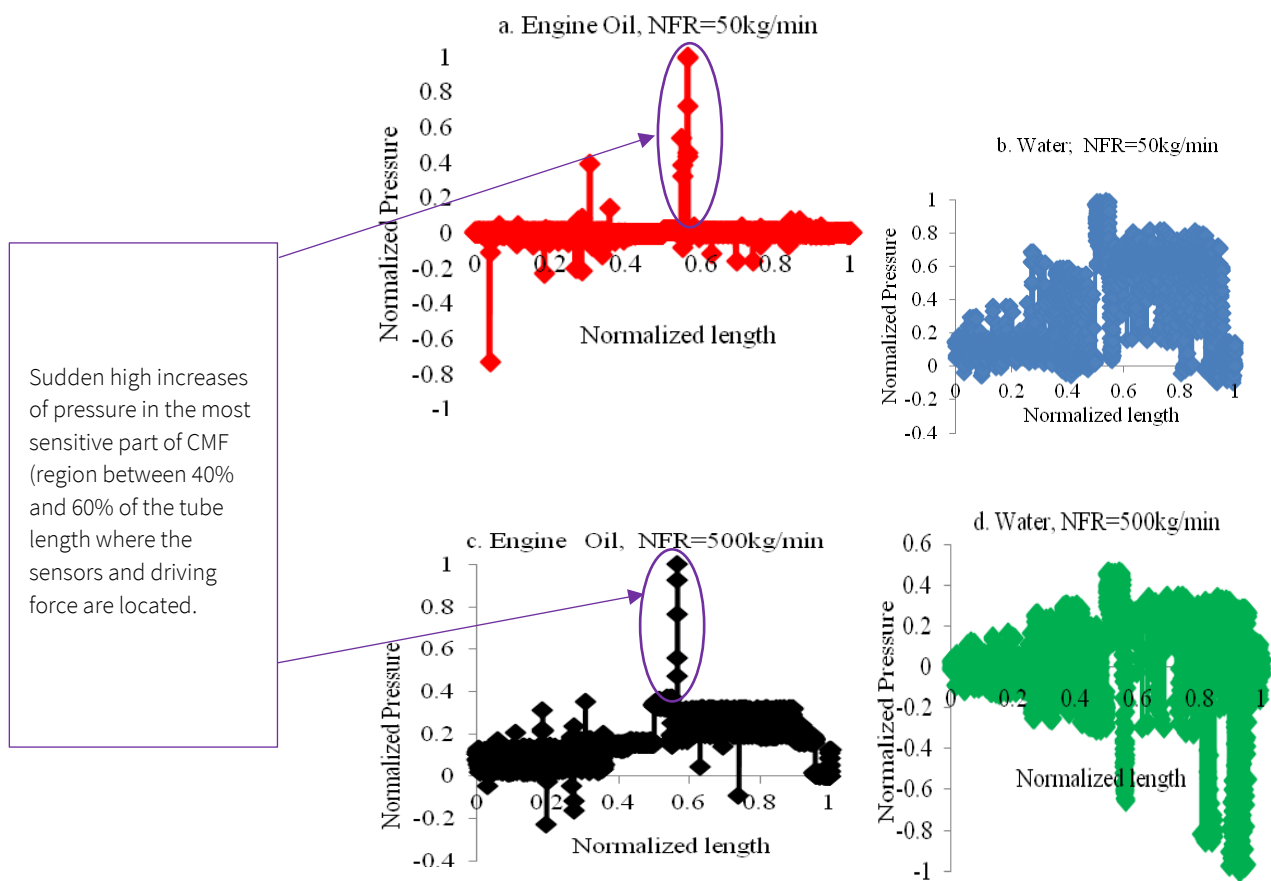
Sudden high increases of pressure in the most sensitive part of CMF (region between 40% and 60% of the tube length where the sensors and driving force are located.

Figure 3. Pressure distribution on the tube's wall along the CMF tube for fluid of different viscosities at different mass flowrates.

3.3. Secondary flow occurrence

Other than pressure jumps, the secondary flow near the sensors' locations is another (even major) factor of the CMF's error in the measurement of high viscosity flows. Figure 4 to Figure 7 present the flow patterns for water and Engine Oil. In Figure 4 and Figure 6, the streamlines indicate the flow pattern of pure water with dynamic viscosity at 0.001003 kg/m.s at a low nominal flowrate of 50 kg/min and a high nominal flowra-

te of 500 kg/min, respectively. On the other hand, Figure 5 and Figure 7 present the flow pattern for Engine Oil with high viscosity at the same aforementioned nominal mass flowrates. As the figures show, unlike for the low viscosity flows (pure water flow) where the secondary flow does form at the sensors' locations, for the highly viscous flows the secondary/reverse flows occur at the sensors' locations.
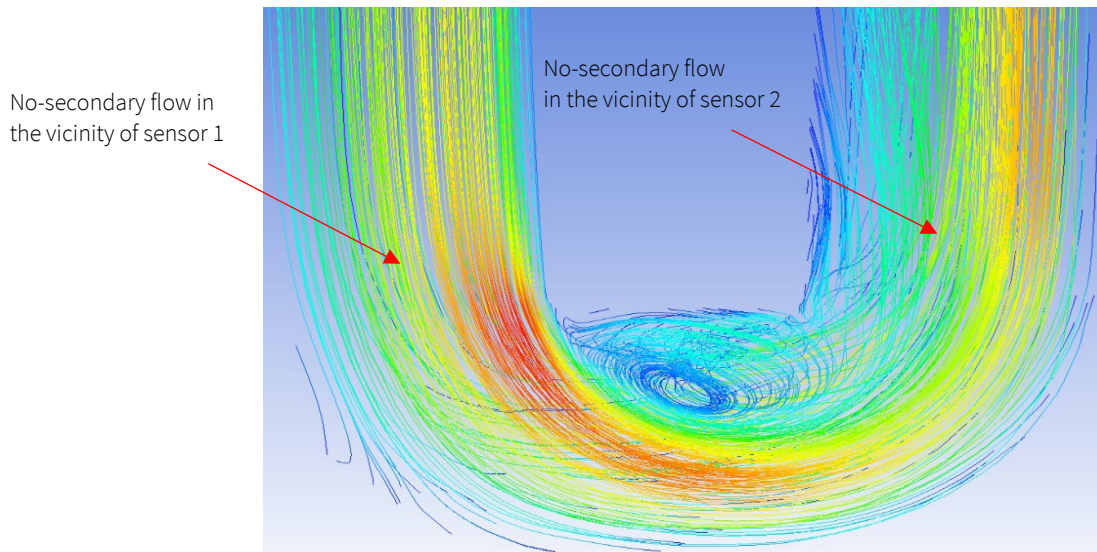

No-secondary flow in the vicinity of sensor 1

No-secondary flow in the vicinity of sensor 2

Figure 4. The flow of water through a CMF at 50kg/min-Streamlines

Secondary flow in the vicinity of sensor 1

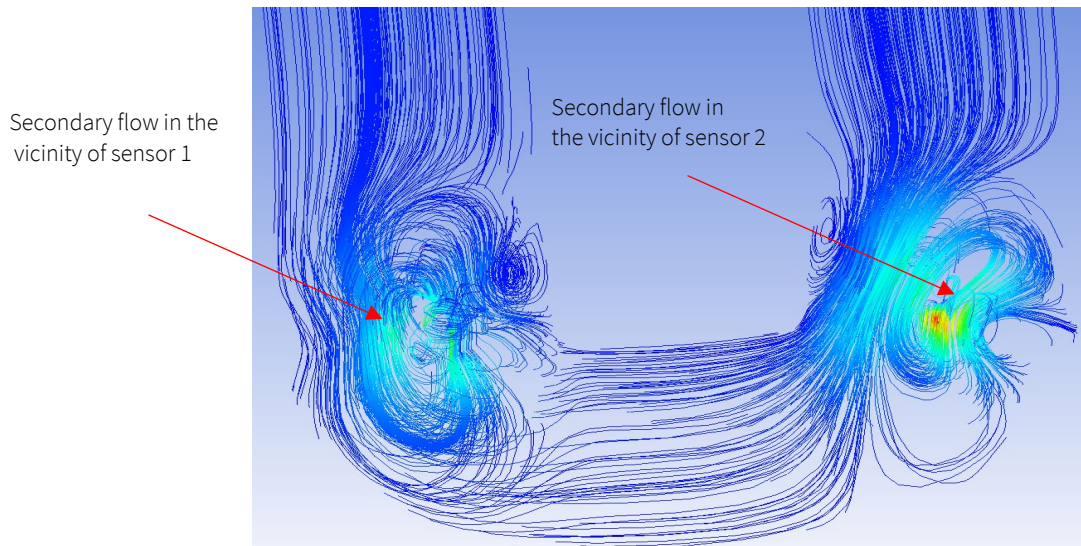Secondary flow in the vicinity of sensor 2

Figure 5. Flow of Engine Oil, dyn-visc=1.06 kg/m.s through a CMF at 50 kg/min

Due to secondary flow occurrence at the sensors' locations, a part of the flow's momentum diminishes in the reversed flow and does not contribute to the tube's deformation. Hence, the deformation of the tube at sensors' locations is reduced, and therefore the CMF model reads lower masses of the fluid than its actual masses, hence large errors. This is supported by the findings of previous studies that also found that the occurrence of secondary flow leads to CMFs' errors (Bobovnik et al., 2004; Kumar & Anklin, 2011; Mole et al., 2008). The difference is that they attributed these errors to low Reynolds numbers only. It is to be noted that the decrease of the Reynolds number for a given fluid through a CMF of constant radius at a given radial speed is due to a change in fluid viscosity. Therefore, one can affirm that the error of CMFs on high viscosity fluid is dependent on fluid viscosity that causes the secondary/reverse flow. This finding is consistent with findings of other research on the measurement of low Reynolds numbers by Coriolis Mass Flowmeters (Huber et al., 2014; Kumar & Anklin, 2011; Rongmo & Jian, 2013).
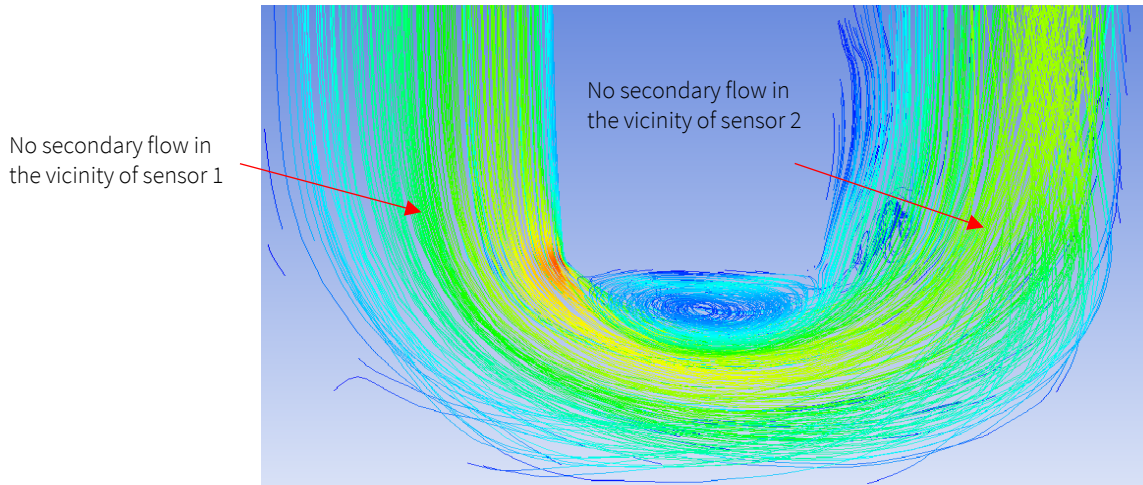

No secondary flow in the vicinity of sensor 1

No secondary flow in the vicinity of sensor 2

Figure 6. Flow of water, dyn_visc= 0.001003 kg/m.s, through a CMF at 500 kg/min

Secondary flow in the vicinity of sensor 1

Secondary flow in the vicinity of sensor 2
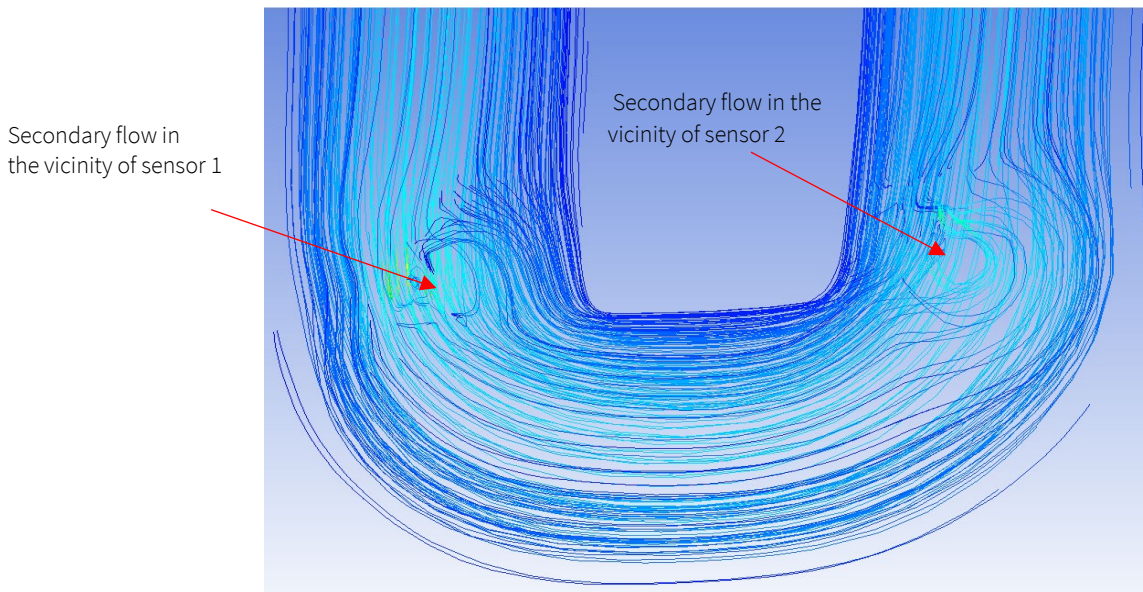
Figure 7. The flow of Engine Oil, dyn_visc=1.06 kg/m.s, through a CMF at 500 kg/min

4. Conclusion and recommendations

This study aimed to characterize the error due to high viscosity through CFD simulations and to explore possible mechanisms that influence that error. This is motivated by the fact that even though CFMs outperform other measurement technologies due to their ability to directly measure mass flowrates, bunker fuels entail high viscosities that are seen to still hinders CMFs accuracy. Moreover, the performance of CMFs on the measurement of high viscosity flow remains less studied. This study analyzed the performance of CMFs on the measurement of high viscosity flow through CFD simulations based on iterative two-ways coupling modeling and describes the possible factors

influencing the error in the measurement of high viscosity flow by CMFs. The two-way FSI has the ability to account for the influences of the dynamics of the fluid domain on the dynamics of the structure domain and vice versa. Hence, it is believed able to produce the most accurate results.

According to the analysis, the errors in measurements grow as the viscosity of the fluid increases or as the mass flowrate of the flow decreases. The study identified two factors that can influence measurement error for highly viscous flows. These are the pressure surge in the vicinity of sensors and the occurrence of secondary flows at sensor locations. From the study, it is found that the secondary flow formation at the sensor locations is the major factor that affects the accuracy of the measurements. When the secondary flow occurs, the inertia force applied to the meter wall reduces. Hence, the tube deformation also reduces. That reduction of tube deformation leads to underestimation of the mass flowrate. For low-viscosity flows, the secondary flow does not occur at the sensors' locations. On the other hand, the steep pressure surge at sensors' locations also causes large CMFs' errors. The high pressure which opposes the exciter's force leads to the underestimation of time shift and hence the mass flowrate, thus leading to high mass flowrates.

The results seem to agree with the results of earlier studies on the occurrence of negative errors that increase as the mass flowrates decrease. The magnitude of error associated with the high viscosity of the fluid being metered found in previous studies has been less than 1.5% (Huber et al., 2017; Kumar & Anklin, 2011). The difference in the error magnitude is likely due to differences in the geometry of CMFs' models. In addition, in this study, a two-way fluid-structure interaction (FSI) coupling was used to account for both the influence of high viscosity on the tube oscillation and flow dynamics on the error. That rigorous simulation of FSI might have permitted quantifying the magnitude of CMFs' error that could not be calculated by using the usual one-way FSI coupling. Further studies about the matter might be needed; not only to validate/complement the current findings but also to possibly

enhance the accuracy of the current model. However, such a model is significantly important since it can serve as a reference for further studies for corrections/compensations of CMFs' error associated with the high viscosity of bunker fuels.

Conflict of interest

The authors have no conflict of interest to declare.

Funding

The authors received no specific funding for this work.

References

Basrawi, Y. F. (2003). Coriolis force mass flow measurement devices. In 49th Int. Instrumentation Symp.(ISA).

Bobovnik, G., Kutin, J., & Bajsić, I. (2004). The effect of flow conditions on the sensitivity of the Coriolis flowmeter. *Flow Measurement and Instrumentation*, *15*(2), 69-76. https://doi.org/10.1016/j.flowmeasinst.2003.12.001

Bobovnik, G., Kutin, J., & Bajsić, I. (2005). Estimation of velocity profile effects in the shell-type Coriolis flowmeter using CFD simulations. *Flow Measurement and Instrumentation*, *16*(6), 365-373. https://doi.org/10.1016/j.flowmeasinst.2005.04.007

Cascetta, F. (1996). Effect of fluid pressure on Coriolis mass flowmeter's performance. *ISA transactions*, *35*(4), 365-370. https://doi.org/10.1016/S0019-0578(96)00048-1

Cascetta, F. (1999). Experimental investigations upon the pressure effects on two Coriolis mass flowmeters of different generation. *ISA transactions*, *38*(2), 149-156. https://doi.org/10.1016/S0019-0578(99)00014-2

Drahm, W., & Bjonnes, H. (2003). A coriolis meter with direct viscosity measurement. *Computing and Control Engineering*, *14*(4), 42-43. https://doi.org/10.1049/cce:20030413

Dutka, A. P., Basker, V. R., Crisalle, O. D., Fricke, A. L., & Kalotay, P. (2004). Evaluation of a capillary-coriolis instrument for on-line viscosity and density measurements of kraft black liquor. *Tappi journal (2002)*, *3*(3), 17-24.

Engelbert, C., Scheulen, R., & Incontri, J. (2007). Successful flow measurement in varnish production. *World Pumps, 2007*(488), 24-25.
https://doi.org/10.1016/S0262-1762(07)70186-4

Gregory, D., West, M., Paton, R., Casimiro, R., Boo, S., Low, Y., Henry, M., Tombs, M., Duta, M., Zhou, F., Zamora, M., Mercado, R., Machacek, M., & Clarke, D. (2008). Two-phase flow metering using a large coriolis mass flow meter applied to ship fuel bunkering. *Measurement and Control*, *41*(7), 208–212.

Hemp, J. (2002). Calculation of the sensitivity of a straight tube Coriolis mass flowmeter with free ends. *Flow measurement and Instrumentation*, *12*(5-6), 411-420.
https://doi.org/10.1016/S0955-5986(01)00031-0

Huber, C., Nuber, M., & Anklin, M. (2014). Effect of Reynolds number in Coriolis flow measurement. In *European Flow Measurement Workshop* (pp. 1-9).

Huber, C., Nuber, M., & Anklin, M. (2017). Accuracy when it counts. why coriolis devices measure reliably in various media properties.

Kalotay, P. (1994). On-line viscosity measurement using Coriolis mass flowmeters. *Flow Measurement and Instrumentation*, *5*(4), 303-308.
https://doi.org/10.1016/0955-5986(94)90035-3

Kalotay, P. (1999). Density and viscosity monitoring systems using Coriolis flow meters. *ISA transactions*, *38*(4), 303-310.
https://doi.org/10.1016/S0019-0578(99)00023-3

Kumar, V., & Anklin, M. (2011). Numerical simulations of Coriolis flow meters for low Reynolds number flows. *Mapan*, *26*(3), 225-235.
https://doi.org/10.1007/s12647-011-0021-6

Kumar, V., Anklin, M., & Schwenter, B. (2010). Fluid-Structure Interaction (FSI) Simulations on the Sensitivity of Coriolis FlowMeter Under Low Reynolds Number Flows. In *Proceedings of the 15th Flow Measurement Conference (FLOMEKO), Taipei, Taiwan* (pp. 13-15).

Kutin, J., Bobovnik, G., Bajsić, I., & Hemp, J. (2005). Modelling and evaluation of velocity profile effects in Coriolis flowmeters. In *Proceedings of 13th International Flow Measurement Conference*.

Kutin, J., & Bajsić, I. (2001). Stability-boundary effect in Coriolis meters. *Flow Measurement and Instrumentation*, *12*(1), 65-73.
https://doi.org/10.1016/S0955-5986(00)00044-3

Kutin, J., Bobovnik, G., Hemp, J., & Bajsić, I. (2006). Velocity profile effects in Coriolis mass flowmeters: Recent findings and open questions. *Flow Measurement and Instrumentation*, *17*(6), 349-358.
https://doi.org/10.1016/j.flowmeasinst.2006.07.005

Mattar, W. (2003). Coriolis metering in difficult industrial applications. *Computing \& Control Engineering Journal*, *14*(4), 44–45.

Mole, N., Bobovnik, G., Kutin, J., Štok, B., & Bajsić, I. (2008). An improved three-dimensional coupled fluid–structure model for Coriolis flowmeters. *Journal of Fluids and Structures*, *24*(4), 559-575.
https://doi.org/10.1016/j.jfluidstructs.2007.10.004

Reizner, J. R. (2005). Batch accuracy: the good, bad and ugly of Coriolis. *InTech Magazine, March*, *7*, 1-4.

Rongmo, L., & Jian, W. (2013). Fluid-structure coupling analysis and simulation of viscosity effect on Coriolis mass flowmeter. In *APCOM & ISCM* (pp. 1-8).

Wang, T., & Hussain, Y. (2010). Pressure effects on Coriolis mass flowmeters. *Flow Measurement and Instrumentation*, *21*(4), 504-510.
https://doi.org/10.1016/j.flowmeasinst.2010.08.001